Photoluminescence line shape in degenerate semiconductor quantum wells

S. K. Lyo and E. D. Jones
Sandia National Laboratories, Albuquerque, New Mexico 87185
(Received 2 March 1988)

A microscopic theory and data are presented for the steady-state photoluminescence line shape at low lattice temperatures in modulation-doped degenerate direct-band-gap semiconductor quantum wells which are excited by a low-intensity cw laser. Electron-hole recombinations occur through direct as well as impurity-assisted (indirect) processes. In our theoretical model the photoluminescence linewidths and spectral shifts arise primarily from ionized-impurity scattering of the majority and minority carriers with smaller contributions from the thermal distribution of the carriers. The dependencies of the line shape on the doping configuration (e.g., space-layer thickness) and the carrier temperature are studied. The theory yields good agreement with the line shape of luminescence data from the modulation-doped n-type and p-type strained $In_xGa_{1-x}/GaAs$ quantum wells with no adjustable parameters.

I. INTRODUCTION

The photoluminescence phenomenon is a powerful tool for studying the electronic properties of semiconductor quantum wells and superlattices. The luminescence has been studied in the presence and absence of magnetic fields.[1-3] In this paper we examine, in the absence of magnetic fields, the microscopic processes responsible for the steady-state photoluminescence line shape at low lattice temperatures in modulation-doped degenerate direct-band-gap semiconductor quantum wells (QW's) which are excited by a low-intensity cw laser. Our interest lies in studying the possibility of using this phenomenon to extract information about the electronic structure, doping configuration, scattering dynamics, and carrier temperature.

In our model, a high-energy low-intensity cw laser creates electron-hole pairs. The laser energy is much larger than the band gap plus the Fermi energy. In n-type materials, for example, the electrons and holes drop rapidly in energy through nonradiative processes to the Fermi surface and top of the valence band, respectively, and reach thermal equilibrium. Radiative recombination occurs between these electron-hole pairs. The electrons and holes in our samples behave like free carriers. This is evidenced by the fact that the slopes in the photon energy versus magnetic field "fan diagram" of our luminescence data for transitions between Landau levels are consistent with the free-carrier model.[2]

The carrier-phonon interactions affect neither the linewidth nor the spectral shift significantly at low phonon temperatures and is not considered. We also ignore effects of neutral-impurity, defect, and surface-roughness scattering. The main role of carrier-carrier interaction is to maintain thermal equilibrium and provide screening. The screening is treated using the random-phase approximation (RPA). Because of screening, band-filling, and lifetime effects, we do not consider excitonic recombinations as confirmed by the absence of an excitonic luminescence peak in our data. Thus, the electrons and holes interact only with the screened Coulomb potentials of the ionized impurities embedded in the barrier regions. It is found that these interactions with ionized impurities fully account for the observed line shapes. While this work treats only the low-lattice-temperature case, the carrier temperature can exceed the lattice temperature depending on the laser intensity.

Thus, the linewidths and spectral shifts arise from ionized-impurity scattering of the majority and minority carriers in our model at low lattice temperatures. The electron-hole recombination occurs through direct as well as impurity-assisted processes. The indirect processes are found to further broaden and shift the line significantly beyond the contributions from the direct process.

In a direct process, an electron and a hole with the same wave vector recombine, emitting a photon as is illustrated in Fig. 1(a). For the case of no impurity broadening, the spectral width arises from the natural widths of the electron and hole states involved as well as from their energy spread originating from the thermal distribution of the minority carriers. For an n-type system, only a small portion of the electrons near the bottom of the conduction band is available for this process, since only a small portion of the states at the top of the valence band is occupied at low temperatures.

The effect of impurity scattering is (a) to broaden the electron and hole levels, thereby causing an uncertainty for the energy conservation condition for direct processes, and (b) to introduce additional higher-order impurity-assisted processes. In an impurity-assisted process, the momentum conservation is broken by allowing the carriers to scatter into intermediate (virtual) states just before or after the photon emission as is illustrated in Fig. 1(b). For this process, even high-energy electrons with energies up to and near the Fermi energy (in n-type systems) can recombine with the holes, emitting high-energy photons. However, because of larger intermediate-energy denominators, the t matrices become smaller with increasing initial energy of the electron, yielding a smaller rate. The interference between the two possible channels each involving an electron- or hole-intermediate state in the indirect process [denoted as paths I and II and represented by directed solid lines in Fig. 1(b)] turns out to subtract intensity from the low-energy side of the pho-

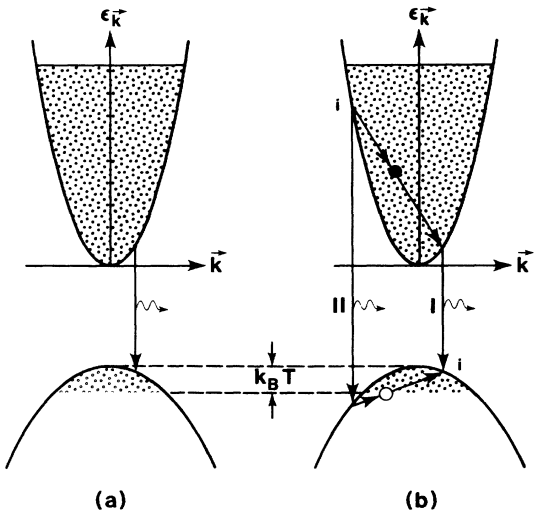

FIG. 1. (a) An electron recombines with a hole with the same wave vector directly emitting a photon (wiggly line). (b) Path I: An electron is scattered into an intermediate virtual state by an impurity (solid circle) and then recombines with a hole. Path II: An electron decays into an intermediate virtual hole via photon emission and then is scattered into a hole by an impurity (open circle). The wave vectors of the initial electron and the final hole are independent. "i" indicates the initial electron and hole states.

tons emitted in the direct process. Therefore the impurity-assisted process yields significant shifting and broadening of the spectral profile.

To summarize, the total linewidth arises from damping effects through the collision-induced widths of the carrier levels, Fermi-level effects through impurity-assisted processes, and temperature effects through the thermal distribution of the minority carriers. Applications are made to the case where the majority carriers are degenerate while the photogenerated minority carriers are nondegenerate. Electrons and holes are assumed to occupy only the ground sublevel and have the same temperature. For convenience the system is assumed to be n type hereafter. The final result is also valid for a p-type system if the parameters for the conduction and valence bands are interchanged.

II. BASIC FORMALISM AND PHOTOLUMINESCENCE LINE SHAPE

The eigenstate of a carrier of type α is given by a plane wave with wave vector $\mathbf{k}$ in the QW plane and the ground-state confinement wave function $\phi_\alpha(z)$. Here z denotes the coordinate perpendicular to the QW. The subscript $\alpha=c$ ($\alpha=v$) will be used for electrons (holes) throughout. The scattering of a carrier by an impurity at $\mathbf{R}_i=(\mathbf{r}_i,z_i)$ is described by[4]

$$\hat{H}_\alpha(\mathbf{R}_i)=s_\alpha \exp(i\mathbf{q}\cdot\mathbf{r}_i)\sum_{\mathbf{k},\mathbf{k}'}\rho_\alpha(q,z_i)V_q a^\dagger_{\alpha\mathbf{k}'}a_{\alpha\mathbf{k}} , \quad (1)$$

where $\mathbf{q}=\mathbf{k}'-\mathbf{k}$, $q=|\mathbf{q}|$, $s_c=-1$ ($s_v=1$) for electrons (holes), and $a^\dagger_{\alpha\mathbf{k}'}$ ($a_{\alpha\mathbf{k}}$) is a second-quantized creation (annihilation) operator. In (1) the quantity V_q equals

$$V_q=\frac{2\pi Ze^2}{\kappa(q+sF_q)} \quad (2)$$

and

$$\rho_\alpha(q,z_i)=\int[\phi_\alpha(z)]^2\exp(-q\,|\,z-z_i\,|\,)dz . \quad (3)$$

The quantities κ, e, Ze, and $s=2m_c^*e^2/\kappa\hbar^2$ in (2) denote the dielectric constant, electronic charge, ionic charge, and two-dimensional RPA screening constant,[5] respectively. The area of the QW is assumed to be unity and m_c^* is the effective mass of the majority carrier. The form factor is given by

$$F_q=\int\int\phi_c(z)^2\phi_c(z')^2\exp(-q\,|\,z-z'\,|\,)dz\,dz' . \quad (4)$$

The line shape is given by the spontaneous recombination rate of the electrons and holes in equilibrium as a function of the emitted photon energy. This rate is formally [cf. Eq. (5)] expressed to second order in the photon field (i.e., using golden rule) and to all orders in other coupling parameters (e.g., carrier-impurity interaction) in the electronic system. The line-shape function is defined as

$$F(\omega)=\frac{-2}{1-e^{\beta\Omega}}\,\mathrm{Im}\Lambda(\omega) , \quad (5a)$$

$$\Lambda(\omega)=\sum_{k,k'}\int_0^\beta\exp(i\omega_r\tau)\times\langle T_\tau a_{ck}(\tau)a_{v-k}(\tau)a^\dagger_{v-k'}a^\dagger_{ck'}\rangle d\tau , \quad (5b)$$

where Im means imaginary part and T_τ is the time ordering operator. The angular brackets denote the thermodynamic average. The quantity $\omega_r=2\pi ri/\beta$ (r is an integer) is to be analytically continued to just above the real axis, namely, $\omega_r\to\Omega+i0=\omega-\mu_c-\mu_v+i0$, where ω is the emitted photon energy minus the band gap, μ_c (μ_v) the electron (hole) chemical potential, and $\beta=(k_BT)^{-1}$. Here k_B and T are Boltzmann's constant and the carrier temperature. The emission rate is obtained by multiplying $F(\omega)/\hbar$ by the square of the band-to-band transition matrix element and summing over photon modes as can be shown readily by evaluating (5) formally in terms of the eigenstates of the interacting system. The photon density of states is assumed to be constant over the energy range of interest. Therefore the function $F(\omega)$ in (5a) is proportional to the emission rate in this approximation and represents the line-shape function.

The direct process discussed in Sec. I is given by the bubble diagram shown in Fig. 2(a):

$$\Lambda_0(\omega)=-2\beta^{-1}\sum_k\sum_l G_{ck}(\zeta_l)G_{v-k}(\omega_r-\zeta_l) , \quad (6)$$

where $\zeta_l=(2l+1)\pi i/\beta$, the factor 2 accounts for the spin degeneracy, l is an integer, and

$$G_{\alpha k}(\zeta_l)=\frac{1}{\zeta_l-\varepsilon^0_{\alpha k}+\mu_\alpha-S_{\alpha k}(\zeta_l+\mu_\alpha)} . \quad (7)$$

Here $\varepsilon^0_{\alpha k}$ is the bare kinetic energy and the self-energy part is given just above the real axis as a sum of the real and imaginary parts:

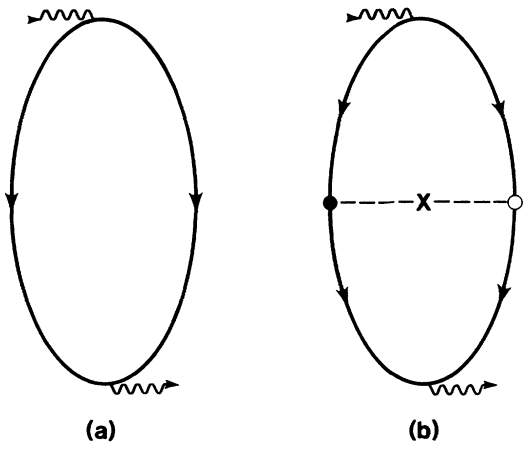

FIG. 2. (a) Bubble diagram for the direct process and (b) one-rung correction for the impurity-assisted process. The solid (open) circle denotes impurity-electron (hole) vertex and the directed lines on the left (right) indicate the electron (hole) propagators. The cross indicates one-impurity averaging. The wiggly lines stand for photon propagators.

$$S_{\alpha k}(\zeta+i0)=M_{\alpha k}(\zeta)-i\Gamma_{\alpha k}(\zeta) . \tag{8}$$

The damping $\Gamma_{\alpha k}$ is responsible for the spectral line broadening and will be evaluated later in a self-consistent Born approximation.

The impurity-assisted process illustrated in Fig. 1(b) is given by the one-rung diagram in Fig. 2(b):

$$\Lambda_1(\omega)=-2\beta^{-1}\sum_{k,k'}U_q^{cv}\sum_l G_{ck}(\zeta_l)G_{v-k}(\omega_r-\zeta_l) \times G_{ck'}(\zeta_l)G_{v-k'}(\omega_r-\zeta_l) , \tag{9}$$

$$U_q^{cv}=s_c s_v N_I V_q^2\int p(z_i)\rho_c(q,z_i)\rho_v(q,z_i)dz_i , \tag{10}$$

where N_I and $p(z_i)$ are the total number and the probability distribution function (normalized to unity) of the ionized impurities, $q=|\mathbf{k}-\mathbf{k}'|$ and $s_c s_v=-1$. Again, the factor 2 in (9) accounts for the spin degeneracy.

To evaluate the line-shape function $F(\omega)$ the l summation in (6) and (9) is converted into a contour integral on the complex plane following a standard technique.[6] After lengthy algebra we find

$$F(\omega)=\frac{4}{\pi}\theta(\omega)\int_0^{\omega}d\zeta\, f(\zeta-\mu_v)f(\omega-\zeta-\mu_c)\left\{\sum_k\frac{\Gamma_{ck}\Gamma_{vk}}{D_{ck}(\omega-\zeta)D_{vk}(\zeta)}-\sum_k\sum_{k'}\frac{2U_q^{cv}(\zeta-\varepsilon_{vk'})\Gamma_{vk}}{D_{ck}(\omega-\zeta)D_{vk}(\zeta)D_{ck'}(\omega-\zeta)D_{vk'}(\zeta)} \times[(\omega-\zeta-\varepsilon_{ck})\Gamma_{ck'}+(\omega-\zeta-\varepsilon_{ck'})\Gamma_{ck}]\right\} , \tag{11}$$

where $f(x)=[\exp(\beta x)+1]^{-1}$ and

$$D_{\alpha k}(\zeta)=(\zeta-\varepsilon_{\alpha k})^2+\Gamma_{\alpha k}^2 . \tag{12}$$

The first and second terms in (11) arise from $\Lambda_0(\omega)$ and $\Lambda_1(\omega)$, respectively, and represent direct and impurity-assisted processes. In (11) and (12) the quantities $\Gamma_{ck''}(\omega-\zeta)$ and $\Gamma_{vk''}(\zeta)$ (with $k''=k,k'$) are approximated as $\Gamma_{\alpha k''}(\varepsilon_{\alpha k''})=\Gamma_{\alpha k''}$ ($\alpha=c,v$), replacing the arguments with their values at the resonances of the denominator in (11). The quantity $\varepsilon_{\alpha k}=\varepsilon_{\alpha k}^0+M_{\alpha k}(\varepsilon_{\alpha k})$ is the renormalized kinetic energy measured from the band edges and ω is now the photon energy minus the renormalized band gap. The product of the Fermi functions in (11) signifies that both the hole state (of energy ζ) and the electron state (of energy $\omega-\zeta$) involved in the recombination process should be thermally occupied. The first term in the large parentheses of (11) is the joint density of states in the presence of collisional broadening of the levels. Terms of the type $(\zeta'-\varepsilon_{\alpha k''})/D_{\alpha k''}(\zeta')$ (with $\zeta'=\zeta$ or $\omega-\zeta$ and $k''=k$ or k') in the second term therein correspond to nonresonant principal values. The unit step function $\theta(\omega)$ in (11) indicates that the photon energies are larger than the band gap. The physics behind the individual processes in (11) was discussed in the Introduction and will not be repeated here.

In the limit of high carrier temperature and weak carrier-impurity interactions (relevant to thick spacer-layer and low-impurity doping), namely, in the limit $k_B T\gg\Gamma_{\alpha k}$, the temperature effect dominates the photoluminescence linewidth. The Lorentzian factors in (11) can be approximated by delta functions yielding for the direct recombination processes [i.e., for the first term in Eq. (11)]

$$F_{\rm dir}^{(0)}(\omega)=4\pi\rho_c\lambda_c\theta(\omega)f(\lambda_v\omega-\mu_v)f(\lambda_c\omega-\mu_c) , \tag{13}$$

where $\lambda_\alpha=\mu^*/m_\alpha^*$, μ^* is the reduced mass, and ρ_α the two-dimensional density of states. The distortion produced in ρ_α near the band edges by interaction with impurities will be ignored. The result in (13) is exact in the absence of any interaction effects, namely for free carriers. The line-shape function in (13) decays initially as a function of ω as $\propto\exp(-\beta\lambda_v\omega)$ and eventually faster as $\propto\exp(-\beta\omega)$ for large ω (i.e., above the band gap plus the Fermi energy). The exponent for the initial decay is larger for a p-type system ($\propto\lambda_c$) than an n-type system ($\propto\lambda_v$) because of the mass difference between electrons and holes: $\lambda_c/\lambda_v=m_h/m_e$ ($\simeq 2$ for the system to be considered later). The physics behind this result will be discussed in Sec. III.

III. APPLICATIONS AND DISCUSSIONS

The QW structure and ionized-impurity distribution profile to be studied is schematically illustrated in Fig. 3. The variational wave functions employed for the ground sublevels are given by

$$\phi_\alpha(z)=\begin{cases} A_\alpha \exp(-\xi_\alpha |z|), & |z| \geq b/2 \\ B_\alpha \cos(\gamma_\alpha z), & |z| < b/2 \end{cases} . \tag{14}$$

The four coefficients A_α, B_α, ξ_α, and γ_α are determined by the conditions that the wave function and its derivative are continuous at the edges of the QW and that the wave function is normalized to unity. The masses are assumed to be the same in the QW and the barriers. The remaining degree of freedom is determined by minimizing the total energy by using, for the many-body energy, the Hartree energy for holes and Hartree and exchange-correlation energies for electrons.[4] For the exchange-correlation potential energy the following expression[7,4] is used:

$$v_{xc}(n(z))=-\frac{0.6109}{r_s}\left[1+0.0545 r_s \ln\left[1+\frac{11.4}{r_s}\right]\right] \times m_c^* e^4/(\kappa\hbar)^2 ,$$

where $n(z)=N\phi_c(z)^2=[4\pi(a_B r_s)^3]^{-1}$, $a_B=\kappa\hbar^2/(m_c^* e^2)$, and N is the two-dimensional carrier density.

The half-width of the levels $\Gamma_{\alpha k}$ is calculated in the self-consistent Born approximation:

$$\Gamma_{\alpha k}=\sum_{k'} \frac{U_q^{\alpha\alpha}\Gamma_{\alpha k'}}{(\varepsilon_{\alpha k}-\varepsilon_{\alpha k'})^2+\Gamma_{\alpha k'}^2} , \tag{15}$$

where $q=|\mathbf{k}'-\mathbf{k}|$. Equation (15) is solved numerically by iteration. The quantity $\Gamma_{\alpha k}$ decreases as a function of energy away from the band edges, reflecting the fact that faster carriers are scattered less by charged impurities. As mentioned earlier, dominant contributions to direct recombination processes arise from the low-energy holes thermally occupied and electrons with the same wave vectors. Therefore, the half-widths $\Gamma_{\alpha k}$ are large for such low-energy carriers, yielding a broad luminescence linewidth. For indirect processes the contributions arise from all energies, although lower-energy states are relatively more important. This fact is in contrast to the dc transport in a degenerate system where only the scattering processes involving high-energy carriers within the thermal layer at the Fermi surface are important.

The form factors for electron-electron [cf., Eq. (4)] and carrier-impurity [cf. Eq. (10)] interactions which enter $U_q^{\alpha\alpha}$ are evaluated in a straightforward way as a function of q using the wave functions in (14). Their expressions are lengthy and tedious and will not be presented here.

Low-temperature photoluminescence data are shown in Fig. 4. The n-type data are from $In_{0.25}Ga_{0.75}/GaAs$ single QW (sample 1) and the p-type data from $In_{0.2}Ga_{0.8}/GaAs$ single QW (sample 2). The characteristics of these samples are shown in Table I. In these systems the QW's are under compression. As a result, the in-plane heavy-hole (i.e., $|\frac{3}{2},\pm\frac{1}{2}\rangle$) bands are split off from the in-plane light-hole (i.e., $|\frac{3}{2},\pm\frac{3}{2}\rangle$) bands by about 60 meV and hence only the latter are occupied. The luminescence line-shape functions obtained from (11) are compared with the data in Figs. 5 and 6 at $T=4$ K for n-type and p-type samples. The theoretical curves are normalized to the data at the peaks of the intensity. Otherwise there is no adjustable parameter. The theoretical band gap corresponds to $\omega=0$ in the figures. The intensity drops rapidly above the Fermi energy (determined from the carrier density and marked by an arrow) approximately over the energy scale of $k_B T$. This is seen

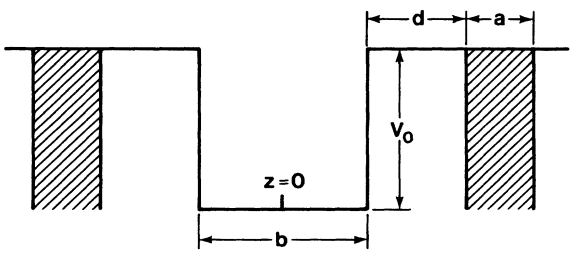

FIG. 3. Symmetric QW of depth V_0. Ionized impurities lie uniformly in the shaded area.

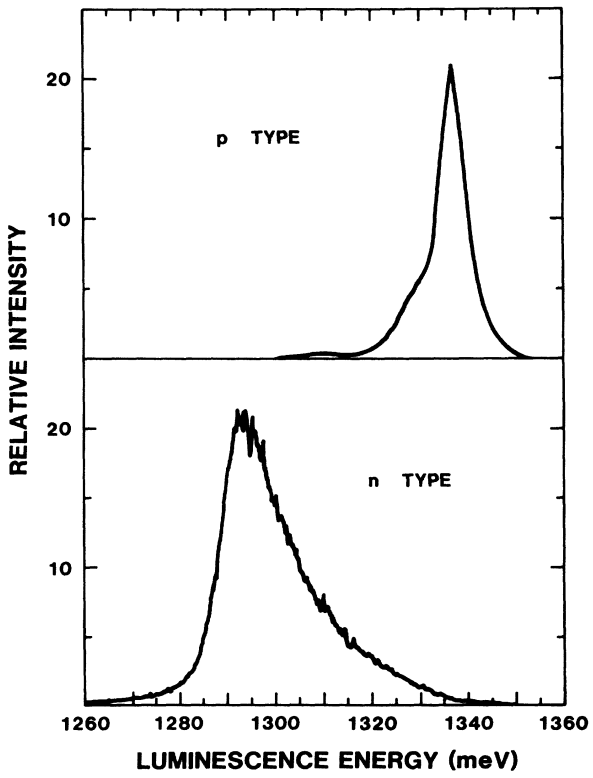

FIG. 4. Low-intensity photoluminescence at the lattice temperature of 4 K excited with an argon-ion laser (514.2-nm) source. The spectral resolution is 1 meV.

TABLE I. The QW structures used for the luminescence line-shape functions displayed in Figs. 5 and 6. The quantities a (calculated from the doping density), b, d, and V_0 are defined in Fig. 3. The in-plane ($m_{\parallel}^*$) are perpendicular ($m_{\perp}^*$) masses are in units of the free-electron mass (Ref. 2). The two-dimensional carrier density N is obtained from magnetotransport measurements.

Type	a (Å)	b (Å)	d (Å)	N (10^{12} cm^{-2})	V_0 (meV)	$m_{\parallel}^*$	$m_{\perp}^*$
n	80	80	10	0.8	160	0.07	0.07
p	19	100	40	0.77	67	0.14	0.35

from (11), where the product of the Fermi functions reduces to $\propto \exp(-\beta\omega)$ for large ω. The carrier temperature equals the lattice temperature (4 K) for the data shown. This conclusion is deduced from the fact that the line shapes remain unchanged as the laser power is further reduced. The line shape for 16 K carrier temperature is also shown for comparison. The low- and high-energy luminescence tails may possibly be due to gap states and donor states in the barriers, respectively, or inhomogeneous broadening, which are not considered in our model.

The dashed curves in Figs. 5 and 6 represent the contributions from the direct processes at 4 K. They rise much more steeply above the band-gap threshold and peak at lower energies than the full results at 4 K. The role of impurity-assisted processes is to broaden and shift the spectral profile to the high-energy side by subtracting the intensity from the low-energy side and adding it to the high-energy region. The full line shapes at 16 K are shown for comparison in Figs. 5 and 6. The line shapes are broader as expected.

The linewidth for the p-type system in Fig. 6 is considerably narrower than that of the n-type system in Fig. 5, although the carrier density (i.e., ionized-impurity density) is similar in both systems. Apart from the obvious reason that the spacer width is thicker for the former case, there are other more interesting general reasons for this difference. The luminescence linewidths are narrower in p-type systems than in n-type systems under a similar condition (e.g., carrier density and QW parameters) essentially because the (in-plane) electron mass is lighter than the hole mass (e.g., $m_e^*/m_h^* \simeq 0.5$ in our strained-layer system). The disparity in linewidth is expected to become more pronounced as the mass ratio de-

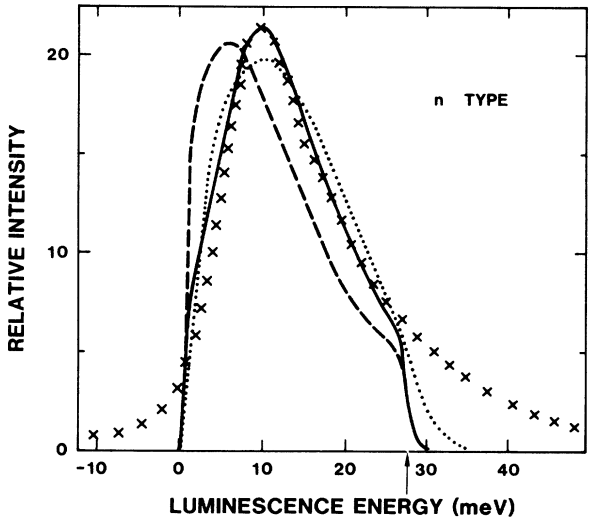

FIG. 5. Full line-shape function (solid curve) at $T=4$ K calculated from (11) and normalized to the intensity peak of the n-type data (crosses) shown in Fig. 4. The parameters used in the calculations are displayed in Table I. The dashed curve denotes the contribution from the direct process only [i.e., the first term of (11)]. The dotted curve indicates the full line shape for $T=16$ K. The origin of the energy axis corresponds to 1284 meV and the arrow denotes the Fermi energy (27.4 meV).

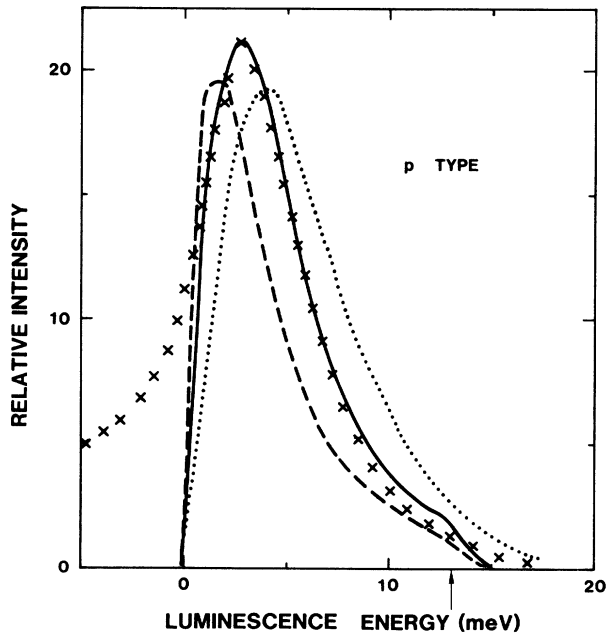

FIG. 6. Comparison of the theoretical line-shape functions with the p-type data shown in Fig. 4. Definitions of the symbols are the same as in Fig. 5. The parameters used in the calculations are displayed in Table I. The origin of the energy axis corresponds to 1334 meV and the arrow denotes the Fermi energy (13.1 meV).

creases. In the following we examine how this different mass affects the linewidths through damping, temperature, and Fermi-energy effects. The screening ($\propto m^*$) is more efficient for a degenerate hole gas (relevant for p type) than an electron gas, yielding smaller damping ($\Gamma_{\alpha k}$), and thus smaller linewidth, for p-type than for n-type systems. This is the dominant effect for the data in Fig. 4. Because of differences in the density of states, a much smaller area in the zone near the Γ point is thermally occupied by (nondegenerate) minority carriers in p-type systems than in n-type systems at the same temperature. This effect is schematically illustrated in Fig. 7. At the same time, the energy spread of the majority carriers available for direct recombinations (indicated by vertical arrows in Fig. 7) with these minority carriers is much smaller in the p type than in the n type, yielding a narrower temperature-induced linewidth. This behavior is clearly reflected in (13). The shift and broadening due to indirect processes is also smaller in the p-type system because the Fermi energy is smaller.

The line-shape functions for various carrier temperatures are displayed in Fig. 8 for an n-type system. They behave similarly for p-type systems. The intensity peaks are normalized to the same point (on the right side of Fig. 8) for an easy comparison by adjusting the intensity scales (marked by multiplicative factors) and shifting the positions of the band-gap threshold (by small amounts) with respect to the line-shape function at 4 K. It is seen that the fit to the data becomes poorer at higher temperatures, thus indicating that the carriers are indeed at the lattice temperature (i.e., 4 K). We also show the line-shape functions obtained from (13) for free carriers. The luminescence threshold on the energy axis for a given temperature is the same for free and interacting cases, while the intensity scale for the former is much larger than that of the latter. It should be noted by comparing the two cases, namely $\Gamma_\alpha=0$ [cf. (13)] and $\Gamma_\alpha\neq0$ in Fig. 8

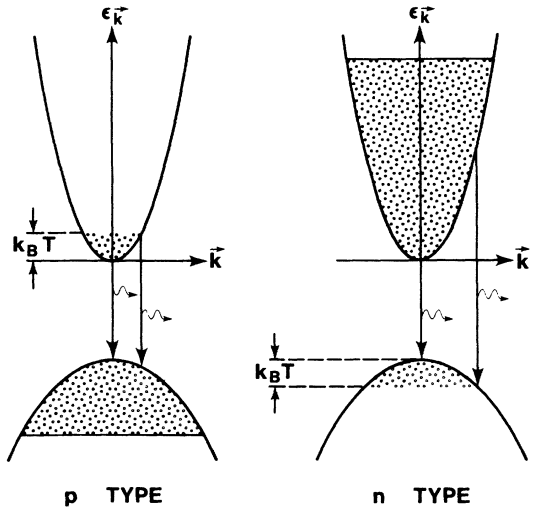

FIG. 7. Schematic illustration of narrower linewidths for p-type systems compared to those of n-type systems due to the temperature effect.

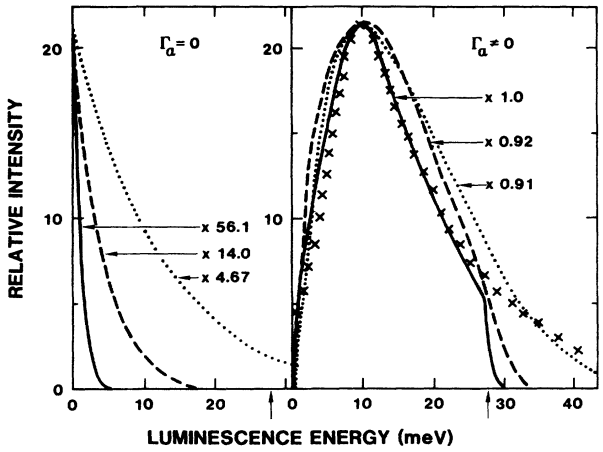

FIG. 8. The full line-shape functions (on the right side) calculated from (11) at the carrier temperatures 4 K (solid curve), 16 K (dashed curve), and 48 K (dotted curve). They are normalized to the n-type data (Fig. 4) at the intensity peak with otherwise the same parameters given in Table I. The curves on the left side are for free carriers. The multiplicative factors denote the scale for the intensity as compared to that of the data. The arrows denote the Fermi energy (27.4 meV).

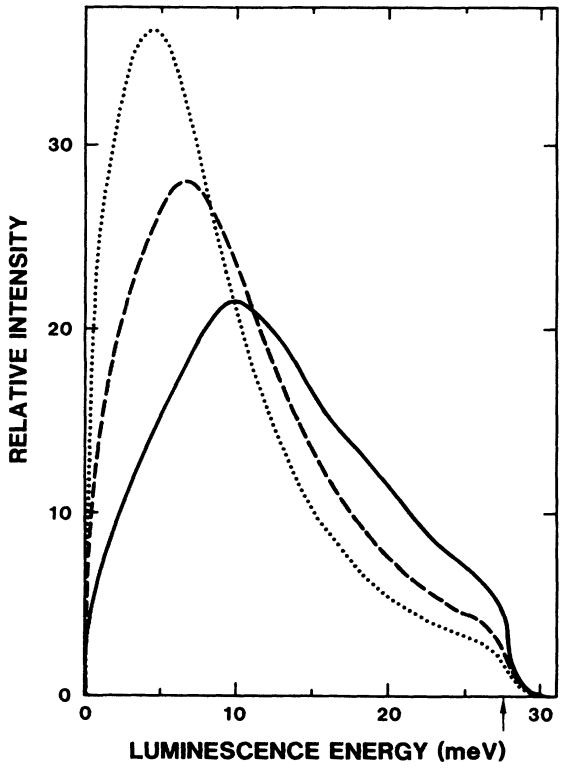

FIG. 9. The full line-shape functions calculated from (11) at $t=4$ K for three spacer thicknesses 10 Å (solid curve), 50 Å (dashed curve), and 100 Å (dotted curve) with the full widths at the half maximum 18, 13.6, and 10.4 meV. The arrow denotes the Fermi energy. Other parameters are the same as those of the n-type system displayed in Table I.

that the slopes in the log intensity versus ω curves for the case $\Gamma_\alpha \neq 0$ below the Fermi energy do not directly reflect the carrier temperatures as one might guess naively, especially for low temperatures. In conclusion our model based on screened impurity scattering alone is seen to explain the global features of the line shape.

The line-shape function is plotted for various spacer-layer thicknesses in Fig. 9. Other QW parameters are the same as given in Table I. The intensity peak shifts to higher energy relative to the band-gap threshold and the linewidth increases as the ionic charges are moved toward the QW.

IV. CONCLUSIONS

A microscopic theory and data were presented for the steady-state photoluminescence line shape at low lattice temperatures in modulation-doped degenerate direct-band-gap semiconductor quantum wells which are excited by a low-intensity cw laser. The spectral profiles of the data, which include the linewidth and the spectral shift, were explained reasonably well in terms of ionized-impurity scattering of the majority and minority carriers. The effect of the thermal distribution of the minority carriers is important only at high carrier temperatures. The electron-hole recombinations occur through direct as well as impurity-assisted processes, the latter leading to further broadening and shifting (to the higher-energy side) of the line. The dependences of the line shape on the carrier temperature and the spacer-layer thickness were studied.

ACKNOWLEDGMENTS

The authors thank Dr. Ian Fritz for providing them with the band-offset data, Dr. T. J. Drummond for a discussion on the quantum-well structure, and Dr. J. E. Schirber for informing them of the magnetotransport data. This work was supported by the U.S. Department of Energy under Contract No. DE-AC04-76DP00789.

[1]J. M. Worlock, A. C. Maciel, A. Petrou, C. H. Perry, R. L. Aggrawal, M. Smith, A. C. Gossard, and W. Wiegmann, Surf. Sci. **142**, 486 (1984).

[2]E. D. Jones, H. Ackermann, J. E. Schirber, T. J. Drummond, L. R. Dawson, and I. J. Fritz, Solid State Commun. **55**, 525 (1985).

[3]A. Petrou, G. Waytena, X. Liu, J. Ralston, and G. Wicks, Superlatt. Microstruct. **3**, 133 (1987).

[4]T. Ando and S. Mori, J. Phys. Soc. Jpn. **47**, 1518 (1979); S. Mori and T. Ando, *ibid.* **48**, 865 (1980).

[5]F. Stern, Phys. Rev. Lett. **18**, 546 (1967).

[6]T. Holstein, Ann. Phys. (N.Y.) **29**, 410 (1964).

[7]O. Gunnarsson and B. I. Lundqvist, Phys. Rev. B **13**, 4274 (1976).